JOURNAL OF SPACECRAFT AND ROCKETS
Vol. 32, No. 5, September–October 1995

Application of Chimera Technique to Projectiles in Relative Motion

Jubaraj Sahu* and Charles J. Nietubicz*
U.S. Army Research Laboratory, Aberdeen Proving Ground, Maryland 21005-5066

This article describes the application of the versatile chimera numerical technique to a time-dependent, multi-body projectile configuration. A computational study was performed to determine the aerodynamics of small cylindrical segments ejected into the wake of a flared projectile. The complexity and uniqueness of this problem result from the segments being in relative motion, embedded in a nonuniform wake flow, and requiring a time-dependent solution. Flowfield computations for this problem have been performed for supersonic conditions. The predicted flowfield over the segments was found to undergo significant changes as the segments separated from the parent projectile. Comparison of the unsteady chimera results with the quasistatic approach shows the difference in drag to be significant, which indicates the need for time-dependent solution techniques. A subsequent experimental program was conducted, and the computed segment positions and velocities were found to be in good agreement with the experimental data.

Nomenclature

C_D = aerodynamic drag
D = projectile diameter (1 caliber)
e = total energy per unit volume
$\hat{F}, \hat{G}, \hat{H}$ = flux vectors in transformed coordinates
J = Jacobian
L = separation distance in calibers
M = Mach number
P = local pressure
$\hat{q}$ = vector of dependent variables
$\hat{S}$ = vector containing viscous terms
t = time
U, V, W = contravariant velocities of the transformed Navier–Stokes equations
u, v, w = Cartesian velocity components of the Navier–Stokes equations
x, y, z = physical Cartesian coordinates
α = angle of attack
γ = ratio of specific heats
κ = molecular and turbulent thermal conductivity
μ = molecular and turbulent viscosity
ξ, η, ζ = transformed coordinates
ρ = density
∞ = freestream conditions

Introduction

AN important parameter in the design of shells and bodies flying in relative motion to each other is the total aerodynamic drag. The base drag constitutes a large part of the total aerodynamic drag, and accurate prediction of the base-region flowfield is necessary. The ability to compute the base-region flowfield for projectile configurations using Navier–Stokes computational techniques has been developed over the past several years.[1,2] Recently, improved numerical predictions have been obtained by using a more advanced zonal upwind flux-split algorithm.[3,4] This zonal scheme preserves the geometry of the base corner, which allows accurate modeling of the base region flow. Previous computational studies have been completed showing the aerodynamic effect for a variety of base geometries. These calculations, however, were performed on standalone projectile configurations and represent a single-body problem. Recently, a multibody problem that involves other bodies flying in the wake of a parent projectile has required computational analyses. This requirement is due in part to the difficulty in finding good experimental and/or analytical data for such problems. The particular problem here is to determine the aerodynamic effect of small cylindrical segments ejected into the wake of a parent projectile. The complexity and uniqueness of this problem results from the trailing segments being in relative motion to each other, embedded in a nonuniform wake flow, and requiring a time-dependent solution. Figure 1 is a spark shadowgraph picture of a recent range test[5] conducted with a number of segments flying in the wake of the parent projectile. Computational results have been obtained by the authors for both the quasisteady case of fixed positions of the segments in the wake[6] and the dynamic case, which involves time-accurate numerical computations. These time-dependent results are the subject of this article.

The time-accurate numerical simulation of multiple aerodynamic bodies in relative motion has been obtained using the chimera[7] approach. This technique has been used to compute inviscid and viscous flows about complex configurations,[8–10] and has been demonstrated for unsteady viscous flow problems with bodies inrelative motion.[11] The chimera approach is a domain decomposition method that uses overset, body-conforming grids and grew out of the necessity to model geometrically complex configurations computationally. The originally developed Navier–Stokes code, zonal F3D,[3] was extended by the authors to include the details of the chimera procedure. This work couples the solution of the Navier–Stokes equations, which govern fluid motion, with the solution to the six-degree-of-freedom (6-DOF) equations of motion. The coupling of the fluid-dynamic solution and rigid-body motion eliminates the need for simplifying assumptions and allows more accurate physically based simulations. This coupling procedure has been used recently by other researchers for store separation problem[12–14] and other moving multiple bodies, including oscillating cylinder and pitching airfoil.[15–17] The applicability of this coupling procedure and the overset grid approach to various store separation cases has been successfully demonstrated in Refs. 12–14. Time-accurate methods were used in Refs. 12 and 14 to predict the trajectory of a finned body released from a generic wing–pylon configuration at transonic speeds. However, the wind-tunnel data that were used for comparison with these computed time-accurate results were not truly time-accurate. A domain decomposition technique was also used in Ref. 18 for a static simulation at a supersonic speed. These computed results depicted the complex interference flowfields between the store and the cavity. The flowfields with the bodies in motion have been shown in Refs. 15 and 16 to be quite different from those computed with the bodies frozen (static). These results show the effects of the dynamics on the interference features, and

---

Received Aug. 1, 1994; revision received April 11, 1995; accepted for publication April 17, 1995.

*Aerospace Engineer. Associate Fellow AIAA.

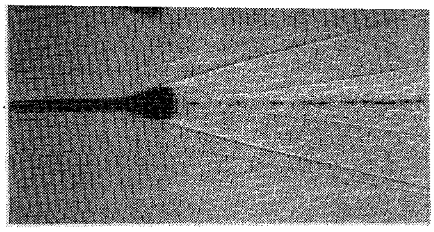

Fig. 1 Spark shadowgraph for multiple segments in the wake of the parent projectile.

indicate the need for time-accurate dynamic numerical simulations for bodies in relative motion. Another example of a static numerical simulation using overlapped grids is given in Ref. 19, which involves an aft-launched projectile separating from the parent carrier. Again, this work, although static in nature, shows the successful use of an overlapped-grid method to a practical wake flow problem. The present work involves the dynamic case of cylindrical segments flying in the wake of a parent projectile and requires time-accurate numerical computations. Its emphasis is on the application of the chimera overlapping-grid approach for accurate numerical calculation of flowfield involving bodies in relative motion.

Governing Equations and Solution Technique

The complete set of time-dependent, Reynolds-averaged, thin-layer Navier–Stokes equations is solved numerically to obtain a solution to this problem. This numerical technique is an implicit finite-difference scheme. Time-accurate calculations are made to numerically simulate the ejection and separation of the segments in the wake of a parent projectile.

Governing Equations

The complete set of three-dimensional time-dependent generalized-geometry Reynolds-averaged thin-layer Navier–Stokes equations for general spatial coordinates ξ, η, and ζ can be written as follows[20]:

$$\partial_\tau \hat{q} + \partial_\xi \hat{F} + \partial_\eta \hat{G} + \partial_\zeta \hat{H} = Re^{-1} \partial_\zeta \hat{S} \tag{1}$$

where

$\xi = \xi(x, y, z, t)$ = longitudinal coordinate
$\eta = \eta(x, y, z, t)$ = circumferential coordinate
$\zeta = \zeta(x, y, z, t)$ = nearly normal coordinate
$\tau = t$ = time

and

$$\hat{q} = \frac{1}{J}\begin{bmatrix} \rho \\ \rho u \\ \rho v \\ \rho w \\ e \end{bmatrix}, \quad \hat{F} = \frac{1}{J}\begin{bmatrix} \rho U \\ \rho u U + \xi_x p \\ \rho v U + \xi_y p \\ \rho w U + \xi_z p \\ (e+p)U - \xi_t p \end{bmatrix}$$

$$\hat{G} = \frac{1}{J}\begin{bmatrix} \rho V \\ \rho u V + \eta_x p \\ \rho v V + \eta_y p \\ \rho w V + \eta_z p \\ (e+p)V - \eta_t P \end{bmatrix}, \quad \hat{H} = \frac{1}{J}\begin{bmatrix} \rho W \\ \rho u W + \zeta_x p \\ \rho v W + \zeta_y p \\ \rho w W + \zeta_z p \\ (e+p)W - \zeta_t P \end{bmatrix} \tag{2}$$

In Eq. (1), the thin-layer approximation is used, and the viscous terms involving velocity gradients in both the longitudinal and circumferential directions are neglected. The viscous terms are retained in the normal direction for the projectile and segments, and are collected into the vector $\hat{S}$. In the wake or the base region, similar viscous terms are also added in the streamwise direction. For this computation, the diffusion coefficients μ and κ contain molecular and turbulent parts. The turbulent contributions are supplied through an algebraic eddy-viscosity turbulence model developed in Ref. 21.

Numerical Technique

The implicit, approximately factored scheme for the thin-layer Navier–Stokes equations using central differencing in the η and ζ directions and upwinding in ξ is written in the following form[22]:

$$\begin{aligned}
&\left[I + i_b h \delta_\xi^b (\hat{A}^+)^n + i_b h \delta_\zeta \hat{C}^n - i_b h Re^{-1} \bar{\delta}_\zeta J^{-1} \hat{M}^n J - i_b D_i|_\zeta\right] \\
&\quad \times \left[I + i_b h \delta_\xi^f (\hat{A}^-)^n + i_b h \delta_\eta \hat{B}^n - i_b D_i|_\eta\right] \Delta \hat{Q}^n \\
&\quad = -i_b \Delta t \left\{\delta_\xi^b\left[(\hat{F}^-)^n - \hat{F}_\infty^+\right] + \delta_\xi^f\left[(\hat{F}^-)^n - \hat{F}_\infty^-\right]\right. \\
&\quad \left. + \delta_\eta\left(\hat{G}^n - \hat{G}_\infty\right) + \delta_\zeta\left(\hat{H}^n - \hat{H}_\infty\right) - Re^{-1}\bar{\delta}_\zeta\left(\hat{S}^n - \hat{S}_\infty\right)\right\} \\
&\quad - i_b D_e(\hat{Q}^n - \hat{Q}_\infty)
\end{aligned} \tag{3}$$

where $h = \Delta t$ or $\Delta t/2$ and the freestream base solution is used. Here, δ is typically a three-point second-order-accurate central difference operator, $\bar{\delta}$ is a midpoint operator used with the viscous terms, and the operators δ_ξ^b and δ_ξ^f are backward and forward three-point difference operators. The flux $\hat{F}$ has been eigensplit, and the matrices $\hat{A}$, $\hat{B}$, $\hat{C}$, and $\hat{M}$ result from local linearization of the fluxes about the previous time level. Here J denotes the Jacobian of the coordinate transformation. Dissipation operators D_e and D_i are used in the central space differencing directions. The smoothing terms used in the present study are of the form

$$D_e|_\eta = (\Delta t) J^{-1}\left[\varepsilon_2 \bar{\delta} \rho(B) \beta \bar{\delta} + \varepsilon_4 \bar{\delta} \frac{\rho(B)}{1+\beta} \bar{\delta}^3\right]\Bigg|_\eta J$$

$$D_i|_\eta = (\Delta t) J^{-1}[\varepsilon_2 \bar{\delta} \rho(B) \beta \bar{\delta} + 2.5 \varepsilon_4 \bar{\delta} \rho(B) \bar{\delta}]|_\eta J$$

where

$$\beta = \frac{|\bar{\delta}^2 P|}{|(1+\delta^2) P|}$$

and where $\rho(B)$ is the true spectral radius of B. The idea here is that the fourth difference will be tuned down near shocks (e.g., as β gets large, the weight on the fourth difference drops, while the second difference tunes up).

Chimera Composite-Grid Scheme

The chimera overset-grid scheme is a domain decomposition approach where a configuration is meshed using a collection of overset grids. This scheme allows each component of the configuration to be gridded separately and overset into a main grid. Overset grids are not required to join in any special way. Usually there is a major grid that covers the entire domain or a grid generated about a dominant body. Minor grids are generated about the rest of the bodies. Because each component grid is generated independently, portions of one grid may be found to lie within the solid boundary contained within another grid. Such points lie outside the computational domain and are excluded from the solution process.

Figures 2 and 3 show an example where the parent projectile grid is a major grid and the segment grid is a minor grid. The segment grid is completely overlapped by the projectile grid, and thus its outer boundary can obtain information by interpolation from the projectile grid. Similar data transfer or communication is needed from the segment grid to the projectile grid. However, a natural outer boundary that overlaps the segment grid does not exist for the projectile grid. The chimera technique creates an artificial boundary

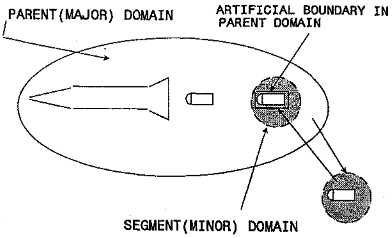

Fig. 2 Intergrid communication.

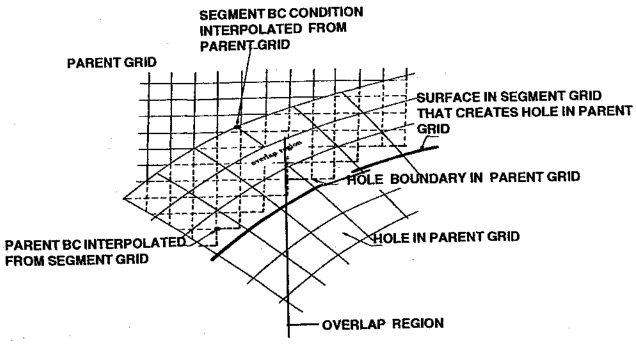

Fig. 3 Overlap region between grids.

(also known as a hole boundary) within the projectile grid, which provides the required path for information transfer from the segment grid to the projectile grid. The resulting hole region is excluded from the flowfield solution in the projectile grid. Equation (3) has been modified for chimera overset grids by the introduction of the flag i_b to achieve that. The i_b array accommodates the possibility of having arbitrary holes in the grid. It is defined so that $i_b = 1$ at normal grid points and $i_b = 0$ at hole points. Thus, when $i_b = 1$, Eq. (3) becomes the standard scheme. But when $i_b = 0$, the algorithm reduces to $\Delta\hat{Q}^n = 0$ or $\hat{Q}^{n+1} = \hat{Q}^n$, leaving $\hat{Q}$ unchanged at hole points. The set of grid points that form the border between the hole points and the normal field points are called intergrid boundary points. These points are updated by interpolating the solution from the overset grid that created the hole. Values of the i_b array and the interpolation coefficients needed for this update are provided by a separate algorithm.[9]

In the present study, which involves multiple bodies in relative motion, the locations of the holes and the intergrid boundary points are time-dependent. Accordingly, the i_b array and the interpolation coefficients are functions of time. This procedure of unsteady chimera decomposition has been successfully demonstrated in Ref. 11. The method depends on three functions: domain connectivity, aerodynamics, and body dynamics. The aerodynamics code depends on the domain connectivity code to supply hole and interpolation information. The domain connectivity code, in turn, depends on the body dynamics code to supply the location and orientation of the moving bodies relative to the primary body. Finally, the body dynamics code depends on the aerodynamics code to provide the aerodynamic forces and moments acting on the moving bodies.

The chimera procedure reduces a complex multibody problem to a number of simpler subproblems. For moving-body problems, all grids are allowed to move with six degrees of freedom relative to an inertial reference frame. Accordingly, bodies can move with respect to others without the necessity of generating new grids. With this composite-overset-grid approach it is thus possible to determine the unsteady relative motion of the segments and associated aerodynamic forces without the need for costly regridding. This procedure also eliminates potential accuracy problems due to severe grid stretching used by many other techniques. The solution procedure is to compute the flowfield at each time step, integrate the pressure and viscous forces for the trailing segments to obtain the drag force and use the predicted drag in a coupled 6-DOF program to compute the new relative position of the trailing segment. At the next time step the solution procedure is repeated for the new position, with the domain decomposition providing all the required interpolation information. Computations are performed on each grid separately. These grids use the available core memory one grid at a time. The remaining grids are stored on an external disk storage device.

Domain Connectivity Function

A major part of the chimera overset-grid approach is the information transfer from one grid into another by means of the intergrid boundary points. Again, these points are the ones that define the hole boundaries and outer boundaries of the minor grids. They depend on the solutions in the overlapping regions. In the present work, the domain connectivity function in three dimensions (DCF3D) code[11] has been used to establish the linkages between the various grids that are required by the flow solver or aerodynamics code described earlier. These linkages include the determination of the interpolation coefficients and the setting up of chimera logic for bodies making holes in overlapping grids. For unsteady-moving-grid cases, this code must be executed at each time iteration. To minimize the computation time, it uses the knowledge of hole and interpolated boundary points at time level n to limit its search regions for finding their corresponding locations at time level $n + 1$.

In general each component grid in an overset grid system represents a curvilinear system of points. However, the positions of all points in all the grids are defined relative to an inertial system of reference. To provide domain connectivity, inverse mappings are used that allow easy conversion from the x, y, z inertial system to ξ, ζ, η computational space. For moving-body problems, these maps for component grids are created only once. Identification of the intergrid boundary points that correspond to the outer boundaries of the minor grids is done simply by specifying appropriate ranges of coordinate indices. The rest of the intergrid boundary points that result from holes created by a body in overset grids are a little more difficult to identify. A collection of analytical shapes such as cones, cylinders, and boxes are used to cut holes in this method.

Boundary Conditions

For simplicity, most of the boundary conditions have been imposed explicitly.[3] An adiabatic wall boundary condition is used on the body surface, and the no-slip boundary condition is used at the wall. The pressure at the wall is calculated by solving a combined momentum equation. Freestream boundary conditions are used at the inflow boundary as well as at the outer boundary. A symmetry boundary condition is imposed at the circumferential edges of the grid, and a simple extrapolation is used at the downstream boundary. A combination of symmetry and extrapolation boundary condition is used at the centerline (axis). Since the freestream flow is supersonic, a nonreflection boundary condition is used at the outer boundary. Similar boundary conditions are used for the segments.

Model Geometry and Computational Grid

The primary or parent projectile is a 10-caliber (1 caliber = diameter at the cylindrical section) cone–cylinder–flare projectile. It consists of a 4.46-caliber conical nose, a 2.82-caliber cylindrical section, and a 3.0-caliber 12.2-deg flare. Figure 4 shows the projectile configuration and the surrounding computational grid for this case, which consists of approximately 20,000 grid points. The grid in the wake region consists of 99 points in the streamwise direction and 119 points in the normal direction. The surface points for each region (body and wake) are selected using an interactive design program. Each grid section was obtained separately and then appended to provide the full grid. The grid for the body region as well as the wake-region was obtained algebraically. An expanded view of the wake-region grid is shown in Fig. 5. The projectile afterbody seen here went through many design changes after the computations were completed, which resulted in the use of a slightly different afterbody in the test firings from that in the computational model. However, because of the large size of the afterbody base compared to the segment, the effect of this change in the afterbody is expected to be minimal on the flowfield over the segments. Figure 5 clearly shows the grid clustering near the base corner of the projectile. Another unique feature of this grid is that the dark band of grid points at the base corner (in the normal direction) slowly opens up with increasing distance downstream of the base. This is an effort to make good use of the grid points and place them in regions of large flow gradients such as the free shear layer in the wake region. The full grid

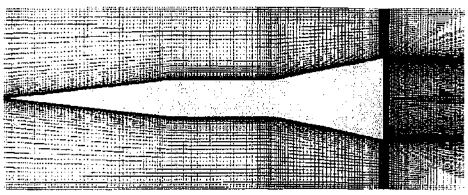

Fig. 4 Computational grid for the parent projectile (major grid).

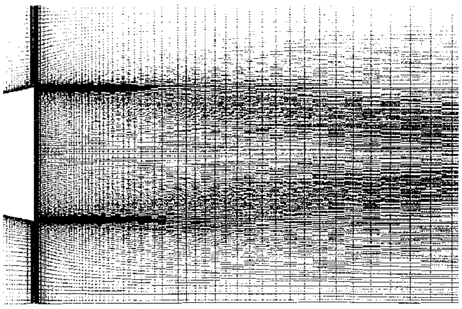

Fig. 5 Expanded view of the base-region grid.

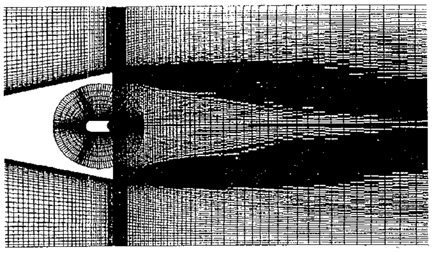

Fig. 6 Segment grid (minor grid) in matted position.

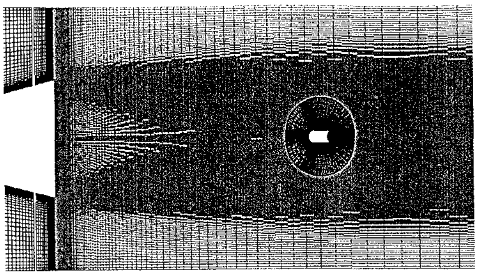

Fig. 7 Segment grid with the segment in wake.

is split into five zones: a small zone in front of the projectile, three zones on the projectile itself, and a wake zone.

The current problem of interest is the effect of the wake of the primary projectile on the small cylindrical body. Each cylindrical segment has a diameter of 9 mm and a length-to-diameter ratio of 2. A typical body-conforming grid for the segment is shown in Fig. 6 and is overset onto the primary projectile grid. This location corresponds to the matted position when the segment is positioned inside of the parent projectile with the aft end of the segment flush with the base of the parent projectile. The segment grid is easily generated independently of the major grid. The grid consists of 101 points in the streamwise direction and 31 points in the normal direction away from the body surface. The chimera technique, as stated earlier, allows individual grids to be generated with any grid topology, thus making the grid generation process easier. For moving-body problems, the segment grid shown in Fig. 6 in the matted position moves with the segment as the segment separates from the parent projectile and moves downstream into the wake (see Fig. 7). Again, there is no need to generate new grids for the segment and/or the parent projectile during the dynamic process.

Results

Time-accurate calculations have been performed to numerically simulate the ejection and separation of the segments in the wake of a parent projectile. Numerical computations were performed for the cases where the parent projectile and one or two segments are in relative motion. The motion of the projectile and the segments is assumed to be confined only to the projectile axis, thus making it an axisymmetric problem. All computations were run at $M_\infty = 4.4$ and $\alpha = 0$ deg, and atmospheric flight conditions were used. The three-plane version of the three-dimensional code was run for the case of 0-deg angle of attack, and, therefore all grids were rotated circumferentially 5 deg on either side of the midplane. This rotation provided the three planes needed in the code to use central finite differences in the circumferential direction.

A converged result was first obtained for the parent projectile alone with the segment in the matted position. Unsteady computations were carried out for the 9-mm segments. In each of these runs, the solution was kept frozen in the first three zones, and computations were made in zone 4 (a small zone upstream of the base) as well as all zones in the wake region only. The frozen solution in zone 3 provided upstream boundary conditions for zone 4. In each case with the segment, the solution was obtained in a time-accurate manner starting with the ejection of the segment into the wake or base region of the parent projectile. These calculations required 15 M words of memory (total memory for all grid zones), and each case used about 60 h of computer time on the Cray X-MP supercomputer. Numerical experiments were made by adding more grid points into the wake region for the static solution and by reducing the time step for part of the dynamic run. More points were added in the streamwise direction, both near the base wall and in the near wake. Computed results were obtained using this new grid for a static case. This calculation gave almost the same base pressure and other flow quantities in the wake as with the original grid. In addition, temporal accuracy, which is important for the dynamic case, was checked by running part of the time-accurate simulation with different time steps. The whole simulation could not be checked for temporal accuracy, because of the large amount of computer time required. A nondimensional time step of 0.005 was used initially, based on Refs. 11 and 12. This time step was reduced to 0.0025, and time-accurate results were obtained for the same time interval of flight. Computed results obtained with the two time steps were quite similar; no significant difference was found between them.

A few qualitative results are presented next, for the one-segment case and the two-segment case. Figure 8 shows the Mach-number contours for the parent projectile with the segment in the matted position. As expected, the shock wave emanating from the nose of the projectile is seen. A strong shock wave is also seen to originate from the cylinder–flare junction. The flow expands at the base corner, which is followed by a recompression shock downstream of the base. As shown in the figure, the outer boundary is placed close to the projectile, and a nonreflection boundary condition procedure is used. The shock waves and the expansion waves pass through this boundary rather smoothly.

Initial system design considerations provided the data used for the ejection velocity of the projectile segments. For the one-segment case, the segment is ejected out from the parent projectile at 92.9 m/s. Figure 9 shows snapshots in time of the Mach-number contours in

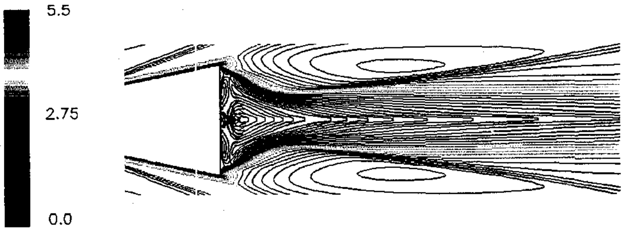

Fig. 8 Mach contours, $M = 4.4$, $\alpha = 0$, segment in matted position.

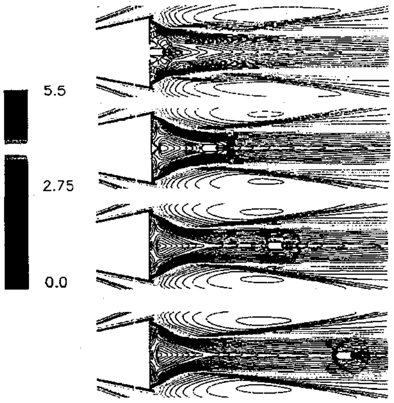

Fig. 9 Mach contours, $M = 4.4$, $\alpha = 0$, segment in various locations in the wake.

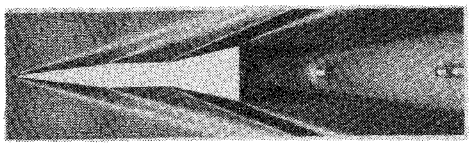

Fig. 10 Computed pressure contours for the entire system, $M_\infty = 4.4$, $\alpha = 0$.

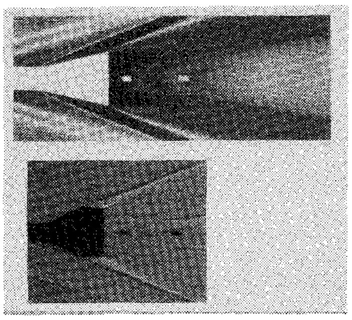

Fig. 11 Comparison of computed pressure contours with spark shadowgraph, $M_\infty = 4.4$, $\alpha = 0$.

the base region for various locations of the segment in the wake. The first picture on the top of this figure corresponds to the case when the segment has just come out of the base of the parent projectile. The other three positions, or locations, correspond to separation distances L of about 2, 4, and 6 calibers from the base of the parent projectile. For $L = 2$, the segment is completely immersed in the subsonic wake of the parent projectile. As seen in this figure for $L = 4$, the flow right in front of the segment is still subsonic. The flow becomes supersonic away from it in the normal direction, and one can see the recompression shock that follows the flow expansions at the base of the parent projectile. As the separation distance is increased to $L = 6$, the flowfield ahead of the segment becomes supersonic. A bow shock wave forms ahead of the segment. As L is increased further, this shock wave becomes stronger. These changes in the flow structure change the pressure on the front face of the segment (the stronger the shock, the higher the pressure) and thus the aerodynamic drag. The overall flowfield behind the segment looks generally the same in all these cases, and the pressure on the back face of the segment does not change significantly.

A set of range tests[5] have been performed for multisegment ejection from the parent projectile. Various configurations with different length-to-diameter ratios and nose radii of the segment were included in the tests. The particular case for which numerical computations have been made corresponds to a length-to-diameter ratio of 2 and a nose radius of 0.5 caliber. Two segments have been numerically simulated. The ejection velocities for these two segments are 52 and 27 m/s for the first (first one to come out) and second segment, respectively. The initial conditions used in the numerical computations for ejection of these segments were obtained from the experimental test results. The second segment was ejected after the first segment was about 1.9 calibers away from the base of the parent projectile. The developed chimera composite-overset-grid approach was used to numerically model this experimental time-dependent separation process.

Figure 10 shows the computed pressure contours for the entire configuration, which includes the parent projectile and the two segments. Seen in this figure are the instantaneous shock wave and the expansion-wave structure when the segments are about 4 and 10 calibers away in the wake. The computational results are now compared with the available experimental results. Figure 11 shows the computed pressure contours in the base region for the two-segment case compared with the experimentally obtained spark shadowgraphs. In this case the second segment is at a separation distance of about 1.25 calibers from the base of the parent projectile. At that time, the first segment is at a separation distance of about 3.8 calibers. As seen in the figure, these locations agree well with the experimental test results. Although not shown here, similar comparisons have also been made for other segment positions further downstream in the wake, indicating good agreement between the computed and experimental results.

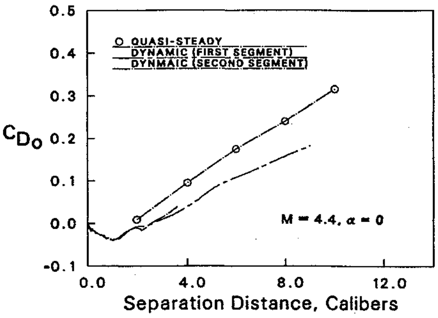

Fig. 12 Drag coefficient (static and dynamic).

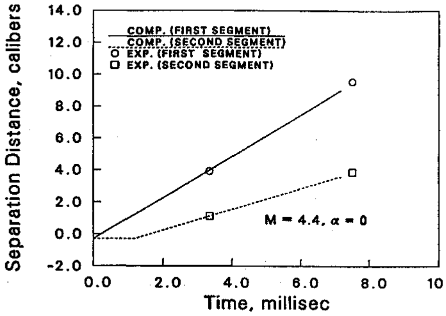

Fig. 13 Separation distance vs time (dynamic).

The entire flowfield over the projectile including the segment is computed to obtain the desired aerodynamics. Surface pressures including the base pressures and the viscous stresses are known from the computed flowfield and can be integrated to give the aerodynamic drag for both parent projectile as well as the cylindrical segments. The drag coefficient for the segments is shown in Fig. 12 as a function of the separation distance. This drag coefficient is based on the area of the segment and the freestream dynamic pressure. As mentioned earlier, for small separation distances ($L < 2$) the segment is submerged in the subsonic wake of the parent projectile. The pressure behind the segment is higher than the pressure ahead of the segment and therefore results in negative drag. As L is increased, the approaching flow to the segment becomes supersonic and a bow shock wave forms in front of the segment. This bow wave increases the pressure at the front face of the segment and results in higher drag. Figure 12 also shows the increase in drag with increasing separation distance.

Also included here are the previously computed[6] quasistatic results obtained for a few locations of the segment in the wake of the parent projectile. These calculations do not take into account the relative motion between the parent body and the segment. As seen in this figure, there is a substantial difference in the predicted drag between the static and the dynamic cases, with the drag being lower for the dynamic case. This highlights the need for time-dependent dynamic solution techniques to accurately simulate problems involving multiple bodies in relative motion.

The drag for the first segment (first one to come out) is shown with a solid line. For the first two calibers of separation distance, both segments essentially follow the same curve. However, for $L > 2.5$, the drag of the first segment is found to be lower than that of the second segment, since it is in the wake of the second segment. Although not shown here, the drag for the parent projectile changes very little in the presence of the small cylindrical segments.

Figures 13 and 14 show the separation distance and the segment velocity as a function of time, respectively. The computed result for the first segment is shown by the solid line and that of the second one by a dashed line. The second segment is ejected about 1.2 ms after the first one. As shown in Fig. 13, the separation distance for the initial matted position of the segments is -0.3 calibers. The computed locations of the segments agree fairly well with the experimentally observed results. Figure 14 shows the comparison of the computed segment velocity (relative to the parent projectile) with the data. For

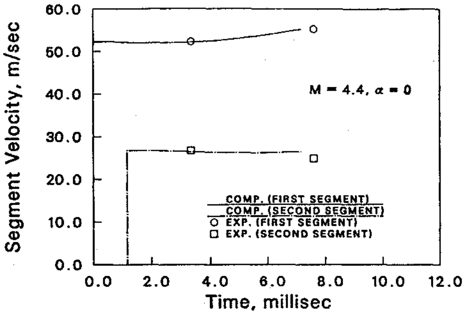

Fig. 14 Segment velocity vs time (dynamic).

the first 2 ms, the segment velocity for the first segment decreases slightly, and then it increases with time. The segment velocity for the second segment decreases only slightly during this time duration. Again, this trend is seen in the experimental results as well.

Concluding Remarks

A computational study has been undertaken to compute the aerodynamics of small cylindrical segments ejected into the wake of a parent projectile. Flowfield computations have been performed at a supersonic Mach number $M_\infty = 4.4$ and $\alpha = 0$ deg using an unsteady, zonal F3D Navier–Stokes code and the chimera composite-grid discretization technique. The computed results show the qualitative features of the base region flowfield for the parent projectile for both the matted position and other positions of the segment in the wake. The predicted flowfield over the small segments was found to undergo significant changes as the segments separated from the parent projectile. For small separation distances the segment experiences negative drag for the dynamic case. With increasing separation distance a bow shock was found to form in front of the segment resulting in higher drag. A significant difference in the predicted drag was observed between the quasisteady and the dynamic simulations. The time-dependent computations were shown to be essential for problems involving relative motion. Comparison of the computed results for the two segments case have been made with the available experimental results, and computed locations, separation distances, and segment velocities were found to be in very good agreement with the experimental results.

This work represents the application of a chimera overlapping-grid approach for accurate numerical calculation of aerodynamics involving multiple bodies in relative motion. The coupling of the fluid-dynamic solution and rigid-body motion eliminates the need for simplifying assumptions and allows more accurate physically based simulations. Together with increased computational resources and the technologies described in this article, multiple design configurations can be accurately simulated and improved multibody systems can be designed more quickly.

References

[1] Sahu, J., Nietubicz, C. J., and Steger, J. L., "Navier–Stokes Computations of Projectile Base Flow With and Without Base Injection," U.S. Army Ballistic Research Lab., BRL-TR-02532, Aberdeen Proving Ground, MD, Nov. 1983 (also see *AIAA Journal*, Vol. 23, No. 9, 1985, pp. 1348–1355).

[2] Sahu, J., "Computations of Supersonic Flow over a Missile Afterbody Containing an Exhaust Jet," *Journal of Spacecraft and Rockets*, Vol. 24, No. 5, 1987, pp. 403–410.

[3] Sahu, J., "Numerical Computations of Transonic Critical Aerodynamic Behavior," *AIAA Journal*, Vol. 28, No. 5, 1990, pp. 807–816 (also BRL-TR-2962, Dec. 1988).

[4] Sahu, J., and Nietubicz, C. J., "Three Dimensional Flow Calculation for a Projectile with Standard and Dome Bases," *Journal of Spacecraft and Rockets*, Vol. 31, No. 1, 1994, pp. 106–112.

[5] von Wahlde, R., private communications, U.S. Army Ballistic Research Lab., Aberdeen Proving Ground, MD, Oct. 1993.

[6] Sahu, J., and Nietubicz, C. J., "A Computational Study of Cylindrical Segments in the Wake of a Projectile," U.S. Army Ballistic Research Lab., BRL-TR-3254, Aberdeen Proving Ground, MD, Aug. 1991.

[7] Steger, J. L., Dougherty, F. C., and Benek, J. A., "A Chimera Grid Scheme," *Advances in Grid Generation*, ASME, edited by K. N. Ghia and U. Ghia, FED-5, American Society of Mechanical Engineers, June 1983.

[8] Atta, E. H., and Vadyak, J., "A Grid Interfacing Zonal Algorithm for Three-Dimensional Flow Transonic Flows About Aircraft Configurations," AIAA Paper 82-1017, 1982.

[9] Benek J. A., Donegan, T. L., and Suhs, N. E., "Extended Chimera Grid Embedding Scheme with Application to Viscous Flows," AIAA Paper 87-1126, Aug. 1987.

[10] Buning, P. G., Chiu, I. T., Obayashi, S., Rizk, Y. M., and Steger, J. L., "Numerical Simulation of the Integrated Space Shuttle Vehicle in Ascent," AIAA Paper 88-4359, Aug. 1988.

[11] Meakin, R. L., "A New Method for Establishing Inter-Grid Communication Among Systems of Overset Grids," AIAA Paper 91-1586, June 1991.

[12] Meakin, R. L., "Computations of the Unsteady Flow About a Generic Wing/Pylon/Finned-Store Configuration," AIAA Paper 92-4568, Aug. 1992.

[13] Lijewski, L. E., and Suhs, N. E., "Chimera-Eagle Store Separation," AIAA Paper 92-4569, Aug. 1992.

[14] Lijewski, L. E., and Suhs, N. E., "A Time-Accurate Computational Fluid Dynamics Approach to Transonic Store Separation of Trajectory Prediction," *Journal of Aircraft*, Vol. 31, No. 4, 1994, pp. 886–891.

[15] Baysal, O., and Yen, G. W., "Kinematic Domain Decomposition for Boundary-Motion-Induced Flow Simulations," *Proceedings of 5th International Symposium on Domain Decomposition Methods for Partial Differential Equations* (Norfolk, VA), Society for Industrial and Applied Mathematics, 1991, pp. 411–419.

[16] Yen, G. W., and Baysal, O., "Computation of Unsteady Flow Past an Oscillating Cylinder Near a Vertical Wall," *Journal of Spacecraft and Rockets*, Vol. 31, No. 4, 1994, pp. 630–635.

[17] Singh, K. P., Newman, J. C., III, and Baysal, O., "Dynamic Unstructured Method for Flows Past Multiple Objects in Relative Motion," AIAA Paper 94-0058, Jan. 1994.

[18] Baysal, O., Fouladi, K., Leung, R. W., and Sheftic, J. S., "Interference Flows Past Cylinder–Fin–Sting–Cavity Assemblies," *Journal of Aircraft*, Vol. 29, No. 2, 1992, pp. 194–202.

[19] Fouladi, K., Baysal, O., and Newman, J. C., III, "Hybrid Domain Decomposition for Configurations with Multiple and Nonsimilar Components," *Proceedings of 5th International Symposium on Domain Decomposition Methods for Partial Differential Equations* (Norfolk, VA), Society for Industrial and Applied Mathematics, 1991, pp. 476–484.

[20] Pulliam, T. H., and Steger, J. L., "On Implicit Finite-Difference Simulations of Three-Dimensional Flow," *AIAA Journal*, Vol. 18, No. 2, 1982, pp. 159–167.

[21] Baldwin, B. S., and Lomax, H., "Thin Layer Approximation and Algebraic Model for Separated Turbulent Flows," AIAA Paper 78-257, Jan. 1978.

[22] Steger, J. L., Ying, S. X., and Schiff, L. B., "A Partially Flux-Split Algorithm for Numerical Simulation of Compressible Inviscid and Viscous Flows," *Proceedings of the Workshop on Computational Fluid Dynamics*, (Univ. of California, Davis), Inst. of Nonlinear Sciences, 1986.

J. Allen
Associate Editor